Solar Energy Materials & Solar Cells 95 (2011) 2341–2346

Contents lists available at ScienceDirect

Solar Energy Materials & Solar Cells

journal homepage: www.elsevier.com/locate/solmat

Influence of the nanoscale structural features on the properties and electronic structure of Al-doped ZnO thin films: An X-ray absorption study

M. Jullien [a,b], D. Horwat [a,*], F. Manzeh [b], R. Escobar Galindo [c], Ph. Bauer [a], J.F. Pierson [a], J.L. Endrino [c]

[a] Institut Jean Lamour, Département CP2S, UMR 7198 CNRS-Nancy-Université-UPV-Metz, Ecole des Mines de Nancy, Parc de Saurupt, CS14234, 54042 Nancy, France
[b] SMR Automotive Systems France S.A. 154, Avenue du Lys, B.P. 5, 77191 Dammarie-Les-Lys Cedex, France
[c] Instituto de Ciencia de Materiales de Madrid, C.S.I.C., Madrid 28049, Spain

ARTICLE INFO

Article history:
Received 22 October 2010
Accepted 4 April 2011
Available online 22 April 2011

Keywords:
Transparent conducting oxide
XANES
Resistivity
Electronic structure
Homologous phase

ABSTRACT

Transparent Al-doped ZnO thin films were deposited by reactive magnetron sputtering with different oxygen flow rates. The electronic resistivity, measured by the 4 point-probe method, is very sensitive to the sample position relative to the magnetron axis: the closer the magnetron from the axis the higher the resistivity. This is more pronounced for the films deposited under higher oxygen flow rate. Neither Rutherford backscattering spectroscopy nor Zn–K edge X-ray absorption near-edge structure (XANES) analyses evidenced any change in chemical composition such as a measurable variation of the oxygen stoichiometry. XANES at the Al–K and O–K edges show that (i) a portion of the aluminum atoms get positioned in octahedral conformation with oxygen, consistent with the formation of an $Al_2O_3(ZnO)_m$ nanolaminate structure, (ii) the films exhibit relaxed O-terminated (0 0 0 1) surfaces with a higher density of empty states in more resistive samples. These two findings are believed to play a significant role on the electrical measurements by dopant deactivation and by creating an insulating barrier at the film surface, respectively.

© 2011 Elsevier B.V. All rights reserved.

1. Introduction

Electro-optical systems such as solar cells and electrochromic systems use transparent conducting oxides (TCO) as electrodes to collect or drive a current, or to apply a voltage. A key property of a TCO thin film electrode is its sheath resistance ruled by the intrinsic conductivity/resistivity of the material. The most widely studied electrode material, when p-type conductivity is not requested, is Indium Tin Oxide (ITO In_2O_3:Sn). The material can achieve a very low resistivity, in the 10^{-4}–$10^{-5}\,\Omega\,cm$ range. Deposition strategies have been developed to synthesize ITO films without heating of the substrate during growth (see for instance [1,2]) but involve high production costs due to the price of indium as well as a high environmental impact because of the lack of recycling procedures of indium and tin. A promising alternative is to dope ZnO, a wide bandgap semiconductor (E_g close to 3.3 eV), with trivalent ions (such as Al^{3+}, Ga^{3+}). It is then possible to generate low, though slightly higher than state of the art ITO, thin film resistivity along with a high transparency in room temperature sputter deposited Al-doped ZnO films [3]. In Al-doped ZnO films efficient n-type doping occurs as neutral Al atoms from the vapor phase position at Zn sites to form Al_{Zn}^{x} structure elements. Al_{Zn}^{x} is a shallow donor, which can free one electron upon ionization

$$Al_{Zn}^{x} \Leftrightarrow Al_{Zn}^{\circ} + e' \quad (1)$$

In addition, the oxygen stoichiometry is often argued to play a significant role to the conductivity of n-type undoped ZnO due to the formation of free electrons to compensate for oxygen vacancies. Nevertheless, this is a deep donor and there are very few stable oxygen vacancies in ZnO [4,5]. Lany and Zunger [5] proposed that optically induced metastable singly charged O° and doubly charged $O^{\circ\circ}$ oxygen vacancies can be optically induced and explain the conductivity and coloration of oxygen deficient ZnO.

In sputtering methods, film growth results mostly from the condensation under non-equilibrium conditions of a vapor of individual atoms at the substrate or film surface. The electrical behavior of sputter-deposited Al-doped ZnO films is very sensitive to the dopant concentration and degrades above an Al content that may correspond to the solubility limit of Al in ZnO of 3–4 at% [6]. Moreover, for a fixed Al content, the conductivity is also highly sensitive to the position of samples during growth either for Al-concentrations below or close to hypothetic solubility limit of Al in ZnO [3,7].

Under equilibrium conditions zinc vacancies V_{Zn}^{x} are formed due to excess of oxygen [8]

$$1/2O_2 \Leftrightarrow O_O^{x} + V_{Zn}^{x} \quad (2)$$

* Corresponding author.
E-mail address: david.horwat@ijl.nancy-universite.fr (D. Horwat).

0927-0248/$ - see front matter © 2011 Elsevier B.V. All rights reserved.
doi:10.1016/j.solmat.2011.04.003

Upon ionization this defect produces (consumes) holes (electrons)

$$V_{Zn}^{x} \Leftrightarrow V'_{Zn} + h^{\circ} \quad (3)$$

$$V'_{Zn} \Leftrightarrow V''_{Zn} + h^{\circ} \quad (4)$$

This is generally accepted as a mechanism to inactivate the aluminum dopant [4,5].

The neutrality condition reads

$$[Al_{Zn}^{\circ}] + [h^{\circ}] + [O^{\circ}] + 2[O^{\circ\circ}] = [V'_{Zn}] + 2[V''_{Zn}] + [e'] \quad (5)$$

Equivalently, and more specific to non-equilibrium conditions owing to thin films grown close to room temperature, the formation of Zn vacancies may be facilitated by the bombardment of thin ZnO by oxygen [9], which is typically stronger on the magnetron axis in a sputtering experiment [10]. Hence, the lateral heterogeneity of conductivity could be understood as a competition between doping and compensation mechanisms (see Eqs. (3) and (4). Yoshioka et al. [11] discovered the nanoscale segregation of Al atoms in heavily Al-doped ZnO that form a so-called $Al_2O_3(ZnO)_m$ "homologous structure". Interestingly, they calculated that the formation of the homologous phase is thermodynamically more favorable than the formation of zinc vacancies [12]. In analogy to $In_2O_3(ZnO)_m$ [13], it consists of a nanolaminate structure of nearly undoped ZnO blocks separated by Al_2O_3-like monolayers. The signature of such a phase has been evidenced recently for Al contents as low as 4 at% [7] and even 1.2 at% Al [14]. Sieber et al. [15] observed the formation of tetragonal Al_2O_3 at the interface between reactively sputter-deposited Al-doped ZnO films and silicon substrates. These different mechanisms may explain the degradations of the electrical behavior by dopant inactivation.

To find out the mechanisms in action, it is relevant to bring information on "bulk" and surface effects in thin films. In the present study, we investigate the influence of chemical composition and local structure on the electronic structure measured by XANES, electronic conductivity and optical properties of sputtered 4 at% Al-doped ZnO films. Special attention is paid to the influence of oxygen stoichiometry and coordination of aluminum on the nanoscale structural features and to the difference between "bulk" and surface features.

2. Experimental procedure

Al-doped ZnO films were prepared on soda lime glass substrates using reactive magnetron sputtering of an Al (4 at%)–Zn target (50-mm diameter). The experimental device is a 30-L sputtering chamber pumped down via a mechanical pump and a diffusion oil pump allowing the base vacuum of 10^{-4} Pa and equipped with one unbalanced magnetron system positioned 50 mm apart from the rotating substrate holder axis. The target-to-substrate distance was set to 50 mm. The samples were positioned at 0, 10, 20 and 30 mm from the target axis. The rotation of the substrate holder (200-mm diameter) allowed achieving good thickness homogeneity over the four samples within a deposition run. The target was sputtered using an Ar–O_2 reactive gas mixture at 0.3 Pa and applying 0.1 A to the target. The argon flow rate was set to 20 standard cubic centimeter per minute (sccm) and the oxygen flow rate (f_{O_2}) was set either at 5 or at 5.5 sccm. The gas mixture was introduced near the periphery of the substrate holder. The deposition time for these two gas compositions was set to 15 and 20 min, respectively, resulting in coating thicknesses close to 100 nm as measured by tactile profilometry. The temperature of the substrate did not exceed 50 °C during deposition as evaluated using thermal level stripes (Thermax®). The chemical composition was determined by Rutherford backscattering spectrometry (RBS) with a 5 MV HVEE Tandetron accelerator sited at the Centro de Micro-Análisis de Materiales at Universidad Autónoma de Madrid. RBS spectra were collected using a 2 MeV He^+ beam. In order to improve the sensitivity to oxygen, experiments at the 3.035 MeV non-Rutherford cross section resonance $^{16}O(\alpha,\alpha)^{16}O$ were also performed. In addition, experiments near the resonance were performed at energies of 3.028, 3.055 and 3.072 MeV to ensure the homogenous oxygen content within the coating. The data were acquired simultaneously with two silicon surface barrier detectors located at scattering angles of 170° with an energy resolution of 14 keV and an ion dose of 5 μC per detector. The aluminum content measured by RBS was around 4 at% in all the deposited samples, independently of the synthesis conditions. The films were characterized using X-ray diffraction (XRD), UV–vis–NIR spectrophotometry in the 200–2700 nm range, four-point probe measurements as well as by X-ray absorption near-edge structure (XANES) measurements at the Zn–K, Al–K and O–K edges. The Zn–K edge was recorded with an energy step width of 1 eV at the KMC-2 beamline of the electron storage ring (BESSY-II) at Helmholtz-Zentrum Berlin, while the Al–K and O–K edges were recorded with an energy step width of 0.1 eV at a spherical grating monochromator (SGM) beamline at the Canadian Light Source.

For Al–K and O–K edges, both the surface-sensitive total electron yield (TEY) and the bulk-sensitive fluorescence yield (FLY) were measured simultaneously under quasi-normal excitation and take off at 45° of the surface for FLY measurements. For reference purposes of XRD and spectrophotometry, pure ZnO films of similar thickness (100 nm) were deposited for 20 min using a 50 mm-diameter Zn target (99.9% of purity) in a reactive atmosphere condition (20/5.5 sccm of Ar/O_2) with the geometrical configuration and current used for the deposition of the Al-doped films.

3. Results

The UV–vis transmission spectra and electrical resistivity of the samples are displayed in Fig. 1a and b. The optical spectra are compared to the typical spectrum of the deposited pure ZnO films. The full optical range is not shown here in order to emphasize the optical absorption in the UV region. Nevertheless, all the films were highly transparent in the visible range without any significant difference between the samples. As the films were synthesized closer to the target axis, the absorption edge shifts towards that of pure ZnO, and it is more marked in films obtained with high oxygen flow rates. This is usually referred as the Burstein–Moss effect, which explains the relationship between the optical bandgap energy and the free carriers density [16,17]. So, according to this hypothesis, the farther the samples from the magnetron axis, the higher the density of free carriers becomes. The electrical resistivity (Fig. 1b) is even more sensitive to the oxygen flow rate. The increase in resistivity while approaching to the magnetron axis is obvious for the two gas flow compositions used, the resistivity increases by a factor of 2.5 for 5 sccm O_2 and about 1800 for 5.5 sccm O_2. Therefore, a very fine tuning of the process gas composition is necessary in order to achieve simultaneously highly transparent and moderately electrically homogeneous films. Such behavior has been recently observed for 2 at% Al-doped films deposited by co-sputtering in a similar reactor [3] where the farthest position from the magnetron axis yielded resistivity values down to $6.6 \times 10^{-4}\,\Omega$ cm. In TCO free carriers are subjected to a plasmon resonance excited by infrared

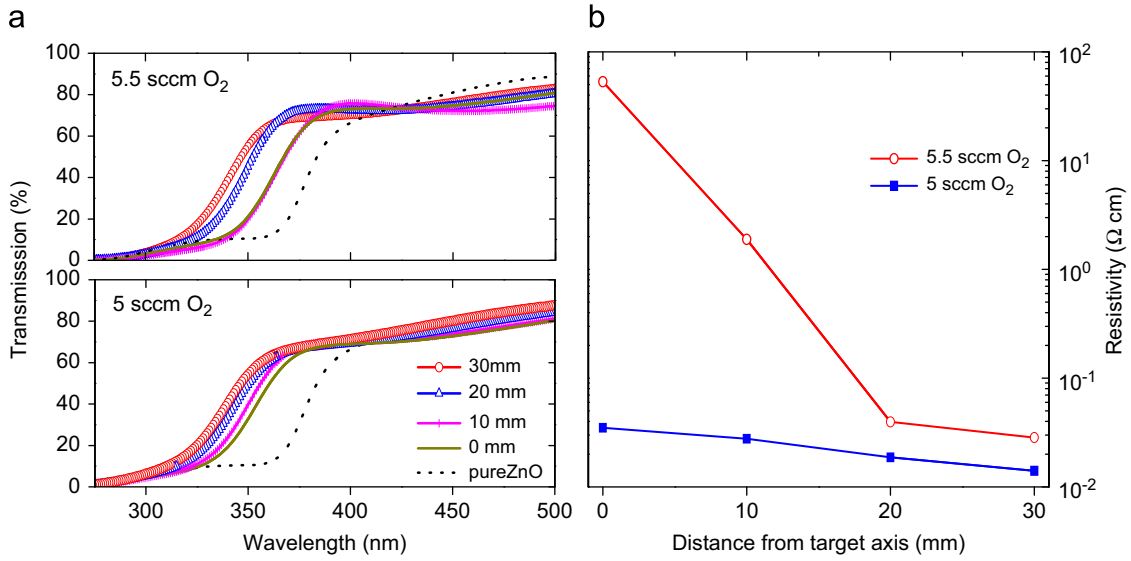

Fig. 1. Optical transmission spectra in the UV range and short wavelengths visible range (a) and resistivity (b) of Al-doped ZnO films reactively sputter deposited with 5 and 5.5 sccm O_2 and placed at different positions from the magnetron axis.

radiations. The plasmon wavelength λ_p is given by

$$\lambda_p = 2\pi c\left(\frac{\varepsilon_\infty \varepsilon_0 m^*}{Ne^2}\right)^{1/2} \quad (6)$$

with N the density and m^* the effective mass of free carriers, ε_∞ the high frequency dielectric constant, ε_0 the permittivity of free space, c the speed of light and e the electron charge. At λ_p a specific absorption of light occurs. As observed from Eq. (6), λ_p shifts towards the visible range as N increases. Detailed discussions on the effect of plasmon resonance on the optical properties of TCO can be found in [18,19]. Fig. 2 displays the visible (long wavelengths, complementary to Fig. 1a) and near infrared (NIR) transmission spectra of the samples deposited for this study. All films deposited with $f_{O_2}=5.5$ sccm exhibit a high transmission in the 500–2700 nm range and the spectra are almost perfectly overlapped. In contrast, for the films deposited with $f_{O_2}=5$ sccm the transmission drops beyond a wavelength which is progressively lowered as the electronic resistivity is low (see Fig. 1b).

The relevant angular region of X-ray diffractograms of all the films are shown in Fig. 3a. All the diffractograms are characteristic of a strong preferential growth along the (0 0 0 2) direction of the ZnO wurtzite structure. Nevertheless, the film deposited using 5 sccm of f_{O_2} and positioned 30 mm from the magnetron axis showed very weak (1 0 $\bar{1}$ 0) and (1 0 $\bar{1}$ 1) diffraction peaks (not shown here) while only the (0 0 0 2) peak was observed for the other conditions. For undoped ZnO (right upper inset of Fig. 3a) the diffracted intensity normalized to the film thickness weakens as the films are positioned closer to the magnetron axis. In parallel, the peak shifts towards lower diffraction angles corresponding to a larger c-axis parameter of the wurtzite cell. The Al-doped films show a very different behavior. While the peak tends to shift towards lower diffraction angles with lower distances from the magnetron axis, as for the undoped case, the peak intensity tends to increase. This effect is much more pronounced and obvious for the highest oxygen flow rate samples. Fig. 3b illustrates a possible correlation between the resistivity and the normalized diffracted intensity. The resistivity is observed to increase strongly as the diffracted intensity raises. This is in strong disagreement with other observations [20] showing that higher crystallinity lowers the resistivity of Al-doped ZnO films.

The XANES study focuses on the films synthesized at 5.5 sccm O_2 and positioned at 0 and 30 mm from the magnetron axis, i.e.

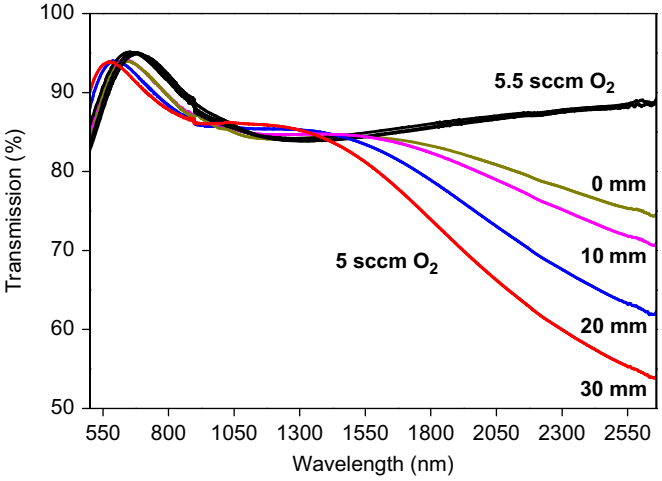

Fig. 2. Optical transmission spectra in the long wavelengths visible range and near infrared range of Al-doped ZnO films reactively sputter deposited with 5 and 5.5 sccm O_2 and placed at different positions from the magnetron axis.

showing very different physical properties. Fig. 4a displays the FLY XANES Zn–K edge spectra of these samples along with the one of a highly absorbent (showing metallic conductivity) and a partially transparent (ZnO_{1-x}, f_{O_2} just below 5 sccm) film shown as reference. The Zn–K edge probes the transition of a Zn 1s electron to Zn 4p empty states. Because of its metallic character, the lineshape of the absorbent film is almost free of features since empty states cannot be detected due to the filling of orbitals. As the oxygen content in the film is increased in the sequence absorbent ⇒ partially transparent ⇒ transparent (5.5 sccm O_2), the features become more pronounced and the absorption edge shifts towards higher energies. The electronic structure is thus strongly sensitive to oxygen stoichiometry. To detect small variations of the oxygen stoichiometry within 1 at% or lower, would request to probe the Zn–K edge by steps below 0.1 eV, which was not possible to reach. Nevertheless, the spectra of the two samples deposited at 5.5 sccm O_2 are almost perfectly overlapped. Fig. 4b plots the RBS $^{16}O(\alpha,\alpha)^{16}O$ oxygen resonance peak of the two samples. In accordance with the XANES at the Zn–K edge, the resonance peaks are very similar. Therefore, the Zn

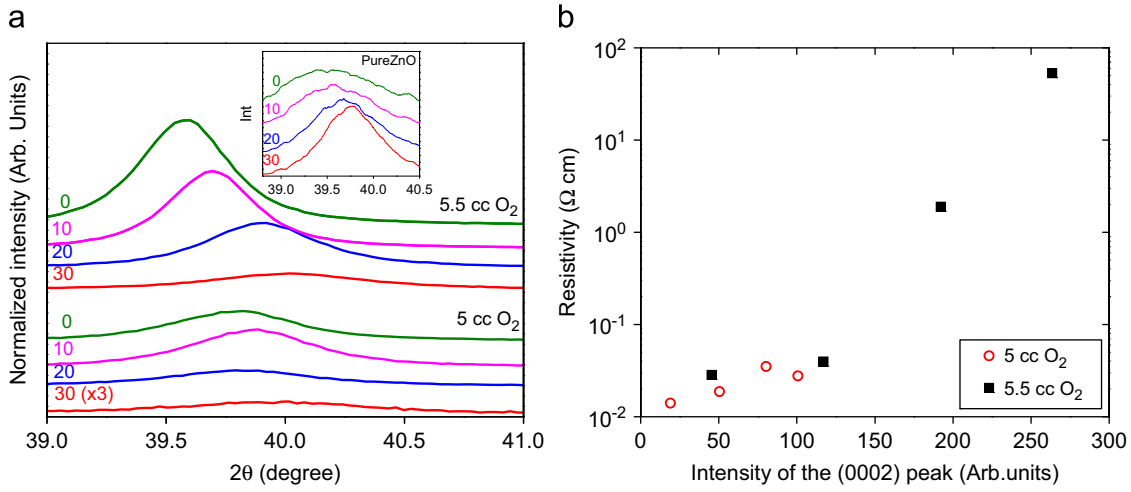

Fig. 3. Details of the X-ray diffractograms (a) and evolution of the resisitivity with the intensity of the (0 0 0 2) diffraction peak of the wurtzite cell (b) of Al-doped ZnO films reactively sputter deposited with 5 and 5.5 sccm O_2 and placed at different positions from the magnetron axis.

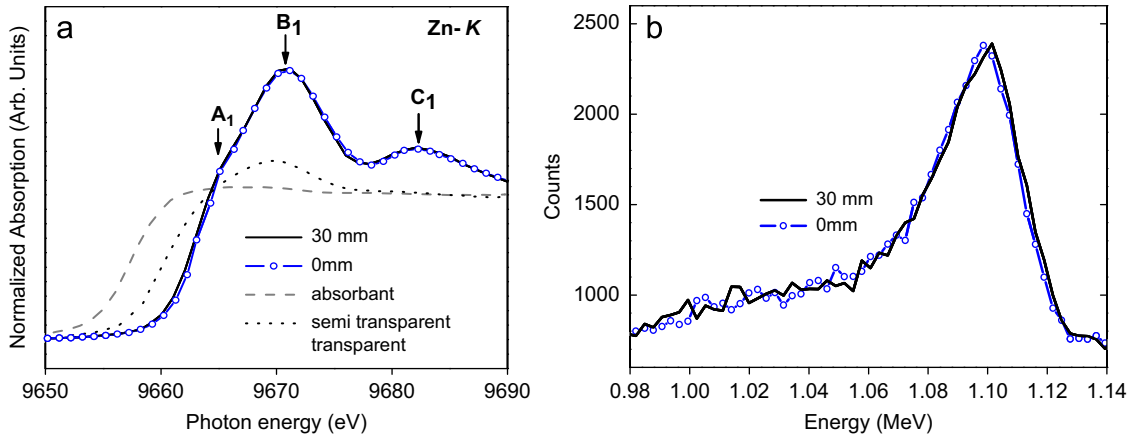

Fig. 4. (a) Zn–K edge XANES of thin Al-doped ZnO films deposited at 0 and 30 mm from the magnetron axis and with 5.5 sccm O_2. The spectra of a highly absorbent and a partially transparent film are indicated as references. (b) RBS $^{16}O(\alpha,\alpha)^{16}O$ oxygen resonance of thin Al-doped ZnO films deposited at 0 and 30 mm from the magnetron axis and with 5.5 sccm O_2.

bonding in the "bulk" of the films and the overall variation in chemical composition seem to be uncorrelated to the variations in electronic conductivity.

Fig. 5 shows the FLY and TEY O–K edge spectra normalized at 565 eV. The O–K edge probes the transition from O 1s electron to O $2p_\pi$ and O $2p_\sigma$ states. Feature C_2 is not observed in undoped ZnO [21] and may originate from the introduction of a 3d character through Al doping. The insets at the right side of Fig. 5 are magnified views of the A_2–D_2 near-edge features after background removal using the best-fitted Gaussian curve; A_2–D_2 were deconvoluted by Gaussian fitting ($\chi^2 < 10^{-4}$). In the FLY mode both the positions of A_2 (535.3 eV), B_2 (537.3 eV), C_2 (538.7 eV), D_2 (540.3 eV) as well as their intensities show little variations for the various samples. This is consistent with the FLY Zn–K edge measurements. The intensities can be sorted in the decreasing order $B_2 > D_2 > A_2 > C_2$. The spectra collected in TEY mode evidence a significant difference between surface and bulk states. Overall, the intensities of the TEY features are higher and show a greater localization. Feature D_2 is here dominant while feature B_2 strongly decayed, which is indicative of O-terminated surface states [21]. If a ZnO monocrystal is cleaved perpendicular to the *c*-axis, it shows (0 0 0 1) O-terminated plane at a side and (0 0 0 $\bar{1}$) Zn-terminated plane at the other side. Here, we should remind that ZnO is a polar material, which does not exhibit surface reconstruction but rather a relaxation of Zn–O bonds [22].

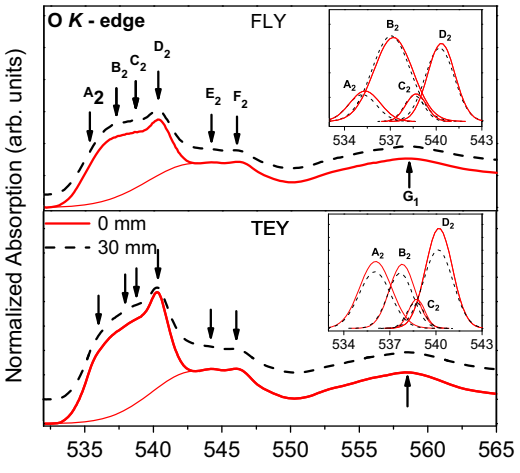

Fig. 5. FLY and TEY O–K edge XANES of Al-doped ZnO films deposited at 0 and 30 mm from the magnetron axis and with 5.5 sccm O_2. The right insets were obtained after background subtraction and Gaussian fitting in the low wavelenghts range.

Feature A_2 is informative about a potential relaxation in the deposited films since it has been proposed to be associated to the hybridization of Zn 4s–O $2p_\sigma$ orbitals corresponding to

σ-type interaction between Zn and O planes in the ZnO crystal [23]. In TEY the intensity of A_2 is much intense than in bulk states and is shifted to higher energies along with B_2, by approx. 0.7 eV. This is in line with the contraction of the first interlayer spacing of O-terminated ZnO surfaces [24]. In contrast to the FLY signal, the TEY intensities of A_2, B_2 and D_2 features are sensitive to the sample position showing that the densities of surface empty states are higher in a more resistive sample.

The Al–K edge XANES allows probing the bonding of Al and was shown recently to enable the detection of aluminum in octahedral coordination with oxygen in Al-doped ZnO films [7,14]. The low energy features of the FLY and TEY Al–K edge spectra presented in Fig. 3 of [7] are displayed in Fig. 6 after subtraction of the background using the best-fit Gaussian curve, followed by a deconvolution by Gaussian fitting (χ^2=approximately 10^{-4}). Features A_3 (1564.6 eV), B_3 (1567 eV) originate from the p–d hybridization splitting of the T_2 orbital of Al in a tetrahedral conformation with oxygen while C_3 (1570 eV) is ascribed mainly to the T_{1u} level of Al in an octahedral conformation with oxygen [23]. Features A_3 and B_3 are expected for Al substituting Zn in the wurtzite structure of ZnO but feature B_3 can only be ascribed to Al in an Al_2O_3-like configuration. Vinnichenko et al. [14] also observed this feature in thin films deposited with thermal assistance and showed it could not be ascribed to the formation of alumina as a second phase but rather to the homologous $Al_2O_3(ZnO)_m$ phase. The XRD signature of the homologous phase is very difficult to differentiate from that of Al-doped ZnO in which Al dopant is activated. Nevertheless, it introduces an expansion of the *c*-axis parameter [24] that can be put in relation to the shift of the (0 0 0 2) diffraction peak of Fig. 4a towards lower diffraction angles as the resistivity increases. The formation of the homologous phase would have the consequence to inactivate a significant portion of the Al dopants, which increases the resistivity of the films. Feature C_3 was detected for the two extreme sample positions but its amplitude is more pronounced in front of the magnetron axis where the measured resistivity is the highest. The signals measured in TEY and FLY modes are very similar showing that the positioning of aluminum in octahedral conformation with oxygen is not a local phenomenon.

4. Discussion

By comparing the XRD signals of Al-doped and undoped ZnO, it is observed that the addition of aluminum into the films did generate a higher crystallinity. This effect has already been reported by Ellmer et al. [10,25]. In contrast, the present analysis pinpoints spatial variations in the crystallinity for films of similar Al and oxygen contents. The dependency of the electrical resistivity to the crystallinity is in the opposite trend to the observations reported for thin films deposited at a fixed position: the films of better crystallinity exhibit a higher resistivity. The activation of Al dopants can be impaired by the compensation with zinc vacancies or, as we proposed recently [7], by the formation of the $Al_2O_3(ZnO)_m$ homologous phase. The formation of alumina may be considered as well [15].

In the present study, it was not possible to detect a significant variation of the chemical composition of samples showing very different resistivity values. The main compensation mechanism of Al doping by zinc vacancies, triggered by energetic oxygen ions, is difficult to discard on the basis of the present results. Even, it seems to be obvious if we consider the strong sensitivity of the electrical resisitivity and density of free carriers *N* to the oxygen flow rate f_{O_2} during the film growth.

Nevertheless, the higher crystallinity of the most resistive films, as evidenced by XRD, is not fully consistent with this hypothesis. Moreover, the increase in the *c*-axis parameter for the more resistive films is consistent with the formation of the homologous phase. In contrast, the increase in *c*-axis parameter in undoped ZnO has been put in relation to the in-plane compressive stresses due to the bombardment of energetic oxygen ions [24]. This is in line with a higher flux of energetic ions for samples positioned on the trajectory facing the magnetron axis in our experimental setup. Based on the dependency of the resistivity to the crystallinity and since the Al dopants are known to improve the crystallization of ZnO, we can discard the formation of a secondary Al_2O_3 phase as the main mechanism for the deactivation of the dopants. Since the films are deposited close to room temperature and without post annealing, their structure results mostly from the condensation process. Hence, it is rather depending on surface than bulk diffusion processes. We propose that grouping of zinc vacancies and aluminum atoms can generate the local conditions to form the homologous phase.

The relaxation of the oxygen terminated surface, as evidenced by O–K edge XANES measurements, may also influence the extraction of charges and application of potential in electro-optical systems, achieved by connecting electrodes to the film surface. In effect, the conduction band of ZnO is dominated by Zn 4s and in a smaller extend by the O 2p and Zn 4p states. Therefore, a high density of derived O 2p empty surface states could result in an insulating surface layer. Thus, in addition to the charges compensation mechanisms, the nanoscale structural phenomena may play an important role in the actual behavior of n-doped ZnO based devices.

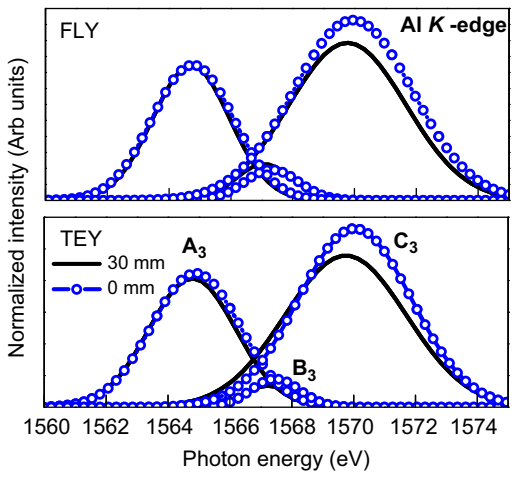

Fig. 6. Relevant features of the FLY and TEY Al–K edge XANES of Al-doped ZnO films deposited at 0 and 30 mm from the magnetron axis and with 5.5 sccm O_2 obtained after background subtraction and Gaussian fitting of the spectra of Fig. 3 of [7].

5. Conclusion

The electronic conductivity and electronic structure of transparent Al-doped ZnO thin films were analyzed in order to isolate chemical and nanoscale structural features influencing the electronic conductivity. The electronic resistivity is higher for samples deposited at high oxygen flow rates and closer to the magnetron axis. Neither Rutherford backscattering spectrometry nor Zn–K edge XANES analyses indicated a change in chemical composition and/or pointed out any variation of the oxygen stoichiometry. XANES at the Al–K and O–K edges show that a portion of the aluminum is positioned in octahedral conformation with oxygen as in an $Al_2O_3(ZnO)_m$ nanolaminate structure. The formation of such a homologous phase was also supported by the X-ray diffraction analyses. It is proposed that the phase forms during the growth process by the grouping of aluminum atoms and zinc

vacancies. XANES O–K revealed that the films exhibit relaxed O-terminated (0 0 0 1) surfaces with a higher density of empty states in more resistive sample. These findings can play a significant role on the electrical measurements due to dopant deactivation and by creating an insulating barrier at the film surface, respectively.

Acknowledgment

The authors thank Dr. Joakim Andersson (Uppsala) for his helpful comments. MJ, DH and FM acknowledge financial support by the Association Nationale de la Recherche et de la Technologie (ANRT). This work was partially supported by MICINN Projects CSD2008-00023 and FIS2009-12964-C05-04. The research performed at the Canadian Light Source is supported by NSERC, NRC, CIHR and the University of Saskatchewan. The synchrotron work at BESSY-II was supported by the EC "Research Infrastructure Action" under the FP6 "Structuring the European Research Area Program" through the "Integrated Infrastructure Initiative Integrating Activity on Synchrotron and Free Electron Laser Science" (Contract no. R II 3-CT-2004-506008).

References

[1] I. Hamberg, C.G. Granqvist, Evaporated Sn-doped In_2O_3 films: basic optical properties and applications to energy-efficient windows, J. Appl. Phys. 60 (1986) R123–R159.
[2] J.R. Bellingham, W.A. Philips, C.J. Adkins, Electrical and optical properties of amorphous indium oxide, J. Phys. Condens. Matter 2 (1990) 6207–6221.
[3] D. Horwat, A. Billard, Effects of substrate position and oxygen gas flow rate on the properties of ZnO: Al films prepared by reactive co-sputtering, Thin Solid Films 515 (2007) 5444–5448.
[4] K. Ellmer, A. Klein, ZnO and its applications, in: K. Ellmer, A. Klein, B. Rech (Eds.), Transparent Conductive Zinc Oxides: Basics and Applications in Thin Films Solar Cells, Springer Series in Materials Science, vol. 104, Springer, Berlin, 2008, pp. 14–19.
[5] S. Lany, A. Zunger, Dopability, intrinsic conductivity, and nonstoichiometry of transparent conducting oxides, Phys. Rev. Lett. 98 (2007) 045501.
[6] S. Cornelius, M. Vinnichenko, N. Shevchenko, A. Rogozin, A. Kolitsch, W. Möller, Achieving high free electron mobility in ZnO:Al thin films grown by reactive pulsed magnetron sputtering, Appl. Phys. Lett. 94 (2009) 042103.
[7] D. Horwat, M. Jullien, F. Capon, J.F. Pierson, J. Andersson, J.L. Endrino, On the deactivation of the dopant and electronic structure in reactively sputtered transparent Al-doped ZnO thin films, J. Phys. D: Appl. Phys 43 (2010) 132003.
[8] F.A. KrÖger, ZnO, in: The Chemistry of Imperfect Crystals, North-Holland, Amsterdam, 1964, pp. 691–701.
[9] T.V. Butkhuzi, A.V. Bureyev, A.N. Georgobiani, N.P. Kekelidze, T.G. Khulordava, Optical and electrical properties of radical beam gettering epitaxy grown n- and p-type ZnO single crystals, J. Cryst. Growth 117 (1992) 366–369.
[10] K. Ellmer, Magnetron sputtering of transparent conductive zinc oxide: relation between the sputtering parameters and the electronic properties, J. Phys. D: Appl. Phys. 33 (2000) R17–R32.
[11] S. Yoshioka, K. Toyoura, F. Oba, A. Kuwabara, K. Matsunaga, I. Tanaka, First-principles investigation of $R_2O_3(ZnO)_3$ (R=Al, Ga, and In) in homologous series of compounds, J. Solid State Chem. 181 (2008) 137–142.
[12] S. Yoshioka, F. Oba, R. Huang, I. Tanaka, T. Mizogushi, T. Yamamoto, Atomic structures of supersaturated ZnO–Al_2O_3 solid solutions, J. Appl. Phys. 103 (2008) 014309.
[13] H. Kasper, Neuartige Phasen mit wurtzitähnlichen Strukturen im System ZnO–In_2O_3, Z. Anorg. Allg. Chem. 349 (1967) 113–123.
[14] M. Vinnichenko, R. Gago, S. Cornelius, N. Shevchenko, A. Rogozin, A. Kolitsch, F. Munnik, W. Möller, Establishing the mechanism of thermally induced degradation of ZnO:Al electrical properties using synchrotron radiation, Appl. Phys. Lett. 96 (2010) 141907.
[15] I. Sieber, N. Wanderka, I. Urban, E. Schierhorn, F. Fenske, W. Fuhs, Electron microscopic characterization of reactively sputtered ZnO films with different Al-doping levels, Thin Solid Films 330 (1998) 108–113.
[16] E. Burstein, Anomalous optical absorption limit in InSb, Phys. Rev. 93 (1954) 632–633.
[17] I. Hamberg, C.G. Granqvist, K.F. Berggren, B.E. Sernelius, L. Engström, Band-gap widening in heavily Sn-doped In_2O_3, Phys. Rev. B 30 (1984) 3240–3249.
[18] K.L. Chopra, S. Major, D.K. Pandya, Transparent conductors—a status review, Thin Solid Films 102 (1983) 1–46.
[19] Z.C. Jin, I. Hamberg, C.G. Granqvist, Optical properties of sputter-deposited ZnO:Al thin films, J. Appl. Phys. 64 (1988) 5117–5131.
[20] M. Birkholz, B. Selle, F. Fenske, W. Fuhs, Structure–function relationship between preferred orientation of crystallites and electrical resistivity in thin polycrystalline ZnO:Al films, Phys. Rev. B 68 (2003) 205414.
[21] P.J. Møller, S.A. Komolov, E.F. Lazneva, A total current spectroscopy study of metal oxide surfaces: I. Unoccupied electronic states of ZnO and MgO, J. Phys.: Condens. Matter 11 (1999) 9581.
[22] A. Wander, F. Schedin, P. Steadman, A. Norris, R. McGrath, T.S. Turner, G. Thornton, N.M. Harrison, Stability of polar oxide surfaces, Phys. Rev. Lett. 86 (2001) 3811–3814.
[23] J.A. Van Bokhoven, T. Nabi, H. Sambe, D.E. Ramaker, D.C. Koningsberger, Interpretation of the Al K- and LII/III-edges of aluminium oxides: differences between tetrahedral and octahedral Al explained by different local symmetries, J. Phys.: Condens. Matter 13 (2001) 10247.
[24] R. Kaltofen, G. Weise, Influence of low-energy bombardment of an RF magnetron sputtering discharge on texture formation and stress in ZnO films, J. Nucl. Mater. 200 (1993) 375–379.
[25] K. Ellmer, F. Kudella, R. Mientus, R. Schieck, S. Fiechter, Influence of discharge parameters on the layer properties of reactive magnetron sputtered ZnO:Al films, Thin Solid Films 247 (1994) 15–23.